THE ASTROPHYSICAL JOURNAL, 404:576–583, 1993 February 20

VARIATIONS OF THE ULTRAVIOLET Fe II AND BALMER CONTINUUM EMISSION IN THE SEYFERT GALAXY NGC 5548

D. MAOZ,[1] H. NETZER,[2,3] B. M. PETERSON,[4] J. BECHTOLD,[5] R. BERTRAM,[4] N. G. BOCHKAREV,[6] T. E. CARONE,[5,7] M. DIETRICH,[8] A. V. FILIPPENKO,[9] W. KOLLATSCHNY,[8] K. T. KORISTA,[10] A. I. SHAPOVALOVA,[11] J. C. SHIELDS,[4,9] P. S. SMITH,[5] U. THIELE,[12] AND R. M. WAGNER[4]

Received 1992 June 1; accepted 1992 August 25

ABSTRACT

We present measurements of the Balmer continuum/Fe II emission blend (the "small blue bump") between 2160 and 4130 Å in the Seyfert galaxy NGC 5548. The measurements are from spectra obtained as part of the combined space-based and ground-based monitoring program of this object in 1988–1989. An iterative scheme is used to determine and subtract the continuum emission underlying the emission blend so as to obtain a light curve sampled once every 4 days. The small blue bump is an important component of the emission-line cooling, constituting about one third of the line flux in this object. Its flux varies with an amplitude of approximately $\pm 20\%$ about the mean, similar to the amplitude of the Balmer line variations during the same period. Its light curve resembles that of Lyα, with a lag of ~ 10 days behind the continuum variations. The bump variation amplitude is independent of the wavelength interval where it is measured, which indicates that both the Balmer continuum and Fe II emission have comparable variation amplitudes. These results suggest that the Fe II UV multiplets and the Balmer continuum are emitted in the same parts of the broad-line region as most other broad emission lines in this object.

Subject headings: galaxies: individual (NGC 5548) — galaxies: Seyfert — techniques: spectroscopic — ultraviolet: galaxies

1. INTRODUCTION

One of the characteristic features of active galactic nuclei (AGNs) is their broad emission lines. In recent years, these lines have been shown to vary in response to changes in the photoionizing continuum radiation driving them. This has emerged as a powerful tool for mapping the interior regions of these objects (Bahcall, Kozlovski, & Salpeter 1972; Blandford & McKee 1982; Maoz et al. 1991; Krolik et al. 1991; Horne, Welsh, & Peterson 1991). In particular, one exceptional data set has been obtained for the Seyfert galaxy NGC 5548. For 8 months in 1988–1989 it was monitored spectroscopically in the UV (1150–3200 Å) with the *IUE* satellite once every 4 days (Clavel et al. 1991). At the same time, a large network of ground-based observers monitored this object at optical wavelengths on an almost daily basis (Peterson et al. 1991). The source underwent substantial variations during the monitoring period, and the resulting data provide a unique opportunity to study the temporal behavior of all the strong emission lines from 1100 to 7000 Å. Clavel et al. (1991) measured light curves for the UV continuum and for all of the strong UV lines, and Peterson et al. (1991) measured the optical continuum and Hβ light curves. Recently Dietrich et al. (1993) measured additional line fluxes, for Hγ, He I λ5876, Hα, and Fe II and He II λ4686 blends, from the optical data base described by Peterson et al. (1991).

In this paper we supplement the above data with measurements of the blend of Fe II and Balmer continuum emission in the spectral region of $\sim$2160–4130 Å. This emission feature, sometimes called the "small blue bump" (Wills, Netzer, & Wills 1985, hereafter WNW), constitutes a substantial fraction of the total emission-line flux and is important for any comprehensive analysis and modeling of NGC 5548. The measurement is, however, difficult for several reasons, as discussed in detail by WNW: (1) The small blue bump is a blend of thousands of highly broadened lines, which span a large wavelength range; (2) the AGN continuum emission underlying the bump can be defined only near the edges of this large spectral range, and its shape needs to be assumed; (3) the *IUE* data are noisy at several of the wavelengths of interest, in particular at the edges of the spectral ranges covered by each of the satellite's cameras; (4) the long-wavelength part of the bump is near the atmospheric cutoff at 3200 where accurate ground-based spectrophotometry is difficult; (5) only a fraction of the ground-based spectra from the monitoring campaign extend to short ($\sim$3200 Å) wavelengths. These difficulties make measurements of the small blue bump less straightforward than those of the other emission lines, and thus special treatment is required. Measurements of the small blue bump in NGC 5548 during the years 1978–1986 can be found in Wamsteker et al. (1990).

In § 2 we describe the iterative method by which we arrive at a light curve for the small blue bump. In § 3 we briefly analyze the temporal characteristics of the small blue bump flux and summarize our main results. A separate paper will incorporate

[1] Institute for Advanced Study, Princeton, NJ 08540.
[2] Laboratory for High Energy Astrophysics, Goddard Space Flight Center, Greenbelt, MD 20771.
[3] School of Physics and Astronomy, Tel Aviv University, Tel Aviv 69978, Israel.
[4] Department of Astronomy, Ohio State University, Columbus, OH 43210.
[5] Steward Observatory, University of Arizona, Tucson, AZ 85721.
[6] Sternberg Astronomical Institute, University of Moscow, Moscow, Russia.
[7] Space Sciences Laboratory, University of California, Berkeley, CA 94720.
[8] Universitätssternwarte Gottingen, D-3400 Gottingen, Germany.
[9] Department of Astronomy, University of California, Berkeley, CA 94720.
[10] Observatories of the Carnegie Institution of Washington, Pasadena, CA 91101.
[11] Special Astrophysical Observatory, Academy of Sciences, Moscow, Russia.
[12] Max-Planck-Institut für Astronomie, Königstuhl, D-6900 Heidelberg, Germany.

and analyze the results for all the observed emission lines in NGC 5548.

2. MEASUREMENTS

In this investigation we used the GEX-extracted (Reichert et al. 1991) *IUE* spectra described in Clavel et al. (1991). The data were transformed to a linear wavelength scale, and the spectra from the short- and long-wavelength *IUE* cameras (SWP from 1150 to 1980 Å and LWP from 2000 to 3200 Å) were combined. Small wavelength corrections were made as necessary so as to place the strong emission lines at their expected wavelengths. Three epochs were not included in the analysis: No LWP spectrum is available for JD 2,447,609; no SWP spectrum is available for JD 2,447,563; and the spectra obtained on JD 2,447,565 are vignetted (Clavel et al. 1991).

The spectra from the ground-based campaign described by Peterson et al. (1991) are more difficult to deal with because of the inhomogeneity of the data base. Absolute calibration of these data is achieved by making the well-justified assumption that the [O III] λ5007 flux does not vary over the time scale of interest, and thus the optical spectra can be calibrated by scaling each spectrum to have the same [O III] λ5007 flux. The value we adopt for the absolute flux in [O III] λ5007 is 5.39×10^{-13} ergs s^{-1} cm^{-2}; this is the same value used by Peterson et al. (1991), except that the value we quote here is in the observed frame rather than the rest frame of NGC 5548. The remaining problem is that the different aperture geometries used result in different relative amounts of nuclear continuum and starlight from the host galaxy in different spectra, and our adjustment for this effect is described below.

As described by Peterson et al. (1991), it is necessary to adjust the optical fluxes obtained through different apertures by a multiplicative factor (which is always close to unity) to correct the [O III] λ5007 flux, which comes from a partially resolved region (cf. Wanders et al. 1992). We have adjusted the optical fluxes for this effect with the point-source correction factor ϕ as given by Peterson et al. (1991) for each of the data sets used here.

A model for the spectrum of the stellar light from the galaxy surrounding the active nucleus was made by combining a suitably scaled off-nuclear spectrum of NGC 5548 with published measurements of the spectral energy distribution of M32. The off-nuclear spectrum was constructed from long-slit CCD spectra obtained on 1989 July 29 with the UV Schmidt spectrograph on the Shane 3 m telescope at Lick Observatory (Miller & Stone 1987). The spectrograph slit width projected to 3″, and the spectrograph was rotated to the parallactic angle of 62° to guard against the effects of atmospheric dispersion. To obtain an off-nuclear spectrum, the nuclear spectrum was extracted twice from the original image, once with an extraction window (i.e., effective slit length) which projects to 7″.5 and once with an extraction window which projects to 15″.4. In each case the extraction window was centered on the nucleus. That the difference between these two spectra is uncontaminated by nuclear emission from the central source is clear from the absence of any residual broad-line features. There are a few weak very narrow emission lines in the off-nuclear spectrum that have been removed by interpolation. Over at least the spectral range 3900–5500 Å, this off-nuclear spectrum, less the weak emission features, is very similar to the spectrum of M32. Therefore, at wavelengths shorter than ~3900 Å, the model starlight spectral energy distribution was augmented by suitably scaled near-UV and satellite-UV measurements of M32 from O'Connell (1980) and Johnson (1979), respectively. The stellar light fraction of the NGC 5548 spectrum becomes negligibly small at wavelengths shorter than ~3000 Å.

The model starlight spectrum was scaled to have a flux $F_G = 3.37 \times 10^{-15}$ ergs s^{-1} cm^{-2} $Å^{-1}$ at 5100 Å (all wavelengths are expressed in the rest frame of NGC 5548; $z = 0.0174$). This is the starlight flux measured through a 5″ × 7″.6 aperture (Peterson 1991). Then, to properly correct for the varying amounts of stellar contamination in the various apertures used in the optical campaign, the stellar spectrum was scaled by a factor $(1 + G/F_G)$, where G is a correction for the starlight through the different apertures of each of the individual data sets comprising the optical data (Peterson et al. 1991). The values of G are taken from Peterson et al. (1992).

Figure 1 shows part of a "typical" spectrum of NGC 5548. It is the combination of spectra from *IUE* (SWP36264 and LWP15517; Clavel et al. 1991) and a contemporaneous ground-based spectrum (n57660ia; Peterson et al. 1991), after subtraction of the appropriate model starlight spectrum. Following WNW, we chose two line-free continuum windows, on both sides of the small bump, at 1800 and 4200 Å (see below). The figure also shows a power law passing through these line-free points. The emission feature we wish to measure is all the flux above this power law from 2200 to 4200 Å, excluding the Mg II λ2800 line, which sits on top of it.

The spectrum is not representative of the data set as a whole in the sense that only 13 of the ground-based spectra extend shortward to near the atmospheric cutoff at ~3200 Å. This is an obvious problem, since much of the small blue bump is between 3200 Å and the Balmer edge (3646 Å), and in the blend of high-order Balmer lines at ~3700–4200 Å. Therefore, the larger the portion of the bump we wish to measure directly, the fewer the epochs for which we can do it. With only 13 unevenly distributed epochs we cannot obtain the kind of temporal information that we are seeking about the small blue bump. We have therefore chosen the approach of measuring directly

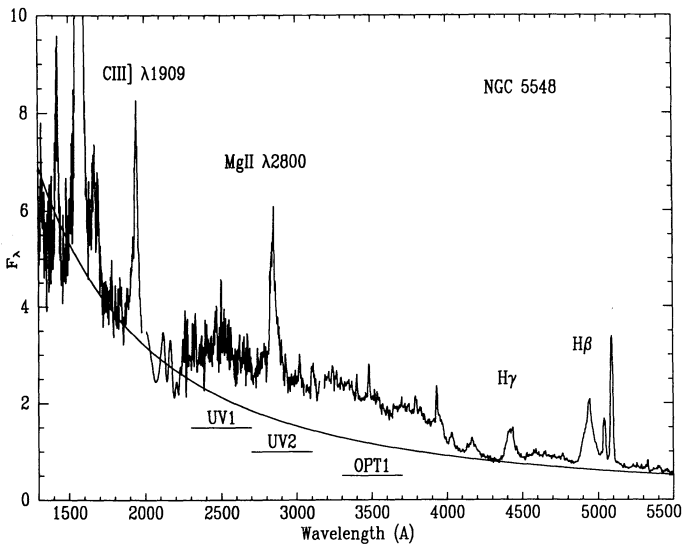

FIG. 1.—Combined UV-optical spectrum of NGC 5548. The solid line is a power law passing through the line-free windows at 1800 and 4200 Å. The small blue bump is the flux above the power law between ~2200 and 4200 Å, excluding the Mg II λ2800 line. Also marked are the UV1, UV2, and OPT1 bands defined in the text. F_λ is in units of 10^{-14} ergs s^{-1} cm^{-2} $Å^{-1}$. The spectrum is as seen in the observer's reference frame.

the flux of the bump only in the *IUE* part of the spectrum, and correcting our measurements by using those spectra that do have complete wavelength coverage, as described below. Since the *IUE* data are sampled every 4 days, we can thus obtain for the small blue bump a light curve that is compatible with the light curves of the other emission lines that have been measured.

The most important element of the measurement is the setting of the underlying AGN continuum (WNW; Wamsteker et al. 1990). We choose to assume that this continuum has a power-law shape with a variable spectral index and amplitude. This is a suitable approximation over the limited wavelength range in which we are interested. To minimize this wavelength range, we set the parameters of the power law using the nearest line-free continuum windows we could define on either side of the bump. On the blue side of the bump we use an 80 Å interval centered at 1800 Å, and on the red side at 4200 Å. The latter is at a sufficiently long wavelength that it can be measured in many (35 separate epochs) of the optical spectra.

For every epoch having a measurement at 4200 Å, the *IUE* observation nearest in time (always within 2 days) was found, and the 1800 Å flux was measured. From the total flux at 4200 Å we then subtracted the value of the stellar flux at 4200 Å derived from the appropriate starlight model, as described above. The power-law continuum spectral index α_ν and amplitude F_0, where $F_\nu = F_0\,\nu^{\alpha_\nu}$, were determined from the corrected fluxes at 1800 and 4200 Å.

In what follows we define three wavelength bands which we use in the small blue bump measurements: UV1 from 2260 to 2655 Å, UV2 from 2655 to 3045 Å, and OPT1 from 3245 to 3635 Å. UV1+2 denotes the combination of the UV1 and UV2 bands. As a first iteration in our measurements, we summed the total flux in the small blue bump in the UV1+2 band (i.e., between 2260 and 3045 Å) above the derived power law in all the *IUE* spectra chosen to match the optical 4200 Å continuum measurements. From the UV1+2 flux we subtracted the Mg II λ2800 flux for each epoch, using the GEX measurements of Clavel et al. (1991). The wavelength range was chosen so as to avoid the edges of the LWP spectra, where the data are particularly noisy. Table 1 gives the results of these measurements. The first two columns give the Julian Date and the starlight-subtracted 4200 Å flux for all epochs for which this optical measurement was feasible. The third and fourth columns give the JD of the nearest *IUE* spectrum and its 1800 Å flux. The fifth column gives the power-law index α_ν determined from the two continuum windows, and the sixth column gives the total flux in the small blue bump above the power law in the UV1+2 band. The seventh column gives, for 13 epochs having these data, the bump flux in the OPT1 band (between 3245 and 3635 Å), where the Balmer continuum is dominant.

TABLE 1

OPTICAL AND UV MEASUREMENTS

JD (opt) (−2440000) (1)	F_λ(4200) (2)	JD (*IUE*) (−2440000) (3)	F_λ(1800) (4)	α_ν 1800–4200 Å (5)	UV1+2 2260–3045 Å (6)	OPT1 3245–3635 Å (7)
7509.....	7.54	7510	3.06	−0.33	5.98	3.04
7524.....	7.78	7522	3.67	−0.15	7.69	2.85
7525.....	8.75	7526	3.59	−0.32	7.78	3.11
7549.....	10.45	7549	3.95	−0.42	6.32	...
7556.....	7.52	7557	3.49	−0.17	7.94	...
7574.....	6.57	7573	2.32	−0.49	6.29	2.29
7576.....	6.25	7577	2.19	−0.50	5.65	...
7583.....	6.44	7581	2.10	−0.59	4.98	...
7587.....	7.56	7586	2.49	−0.58	5.05	...
7590.....	6.51	7590	2.44	−0.43	6.35	...
7592.....	7.80	7590	2.44	−0.64	5.46	2.81
7613.....	10.01	7613	4.10	−0.32	5.15	2.50
7620.....	10.97	7621	4.83	−0.23	6.92	...
7621.....	12.96	7621	4.83	−0.43	5.41	...
7622.....	11.39	7621	4.83	−0.28	6.59	...
7628.....	10.18	7629	4.85	−0.14	7.29	...
7643.....	10.24	7641	4.92	−0.13	7.01	3.49
7645.....	10.99	7645	4.53	−0.31	6.10	...
7655.....	10.29	7653	4.31	−0.29	6.66	...
7658.....	9.84	7657	4.08	−0.31	7.23	...
7660.....	8.66	7661	3.93	−0.20	7.47	3.68
7663.....	9.93	7661	3.93	−0.36	6.48	...
7665.....	9.55	7665	3.81	−0.35	7.02	...
7678.....	6.59	7677	3.16	−0.13	7.66	...
7679.....	8.67	7680	3.18	−0.45	6.50	...
7680.....	6.70	7680	3.18	−0.14	8.02	...
7687.....	8.93	7688	2.60	−0.72	5.09	2.74
7703.....	7.38	7705	2.93	−0.36	5.90	2.45
7711.....	7.94	7709	3.34	−0.29	5.58	...
7716.....	7.68	7717	3.44	−0.21	7.50	2.31
7719.....	8.02	7717	3.44	−0.26	7.23	...
7725.....	8.12	7725	2.94	−0.47	6.38	...
7741.....	5.25	7741	1.65	−0.63	4.54	...
7742.....	3.76	7741	1.65	−0.23	5.62	1.77
7748.....	5.47	7745	1.66	−0.67	4.41	2.47

NOTES.—F_λ(4200) in units of 10^{-15} ergs s^{-1} cm^{-2} Å^{-1}. F_λ(1800) in units of 10^{-14} ergs s^{-1} cm^{-2} Å^{-1}. Fluxes in units of 10^{-12} ergs s^{-1} cm^{-2}.

Included in the latter measurement are all spectra from Peterson et al. (1991) going shortward of 3300 Å (observed wavelength), except for spectra n57614h and n57645ia, both of which are clearly not well flux-calibrated in the far blue part of the spectrum. The flux quoted is the value obtained after subtraction of the starlight model described above.

The small blue bump measurements in Table 1 result in a noisy light curve. Any variations present are comparable to the scatter from point to point. Also, much of the light curve suffers from undersampling. The main source of noise is the optical 4200 Å measurement, which is affected by the heterogeneity of the optical data base and the increasing error in intercalibration of the spectra as one goes away from the [O III] λ5007 line. A small error in this quantity propagates into a large error in the bump flux (see Fig. 1). In an effort to circumvent this difficulty, we have noted that a strong correlation exists between the spectral index α_ν and the 1800 Å flux. Figure 2 shows that the spectrum gets harder as the object brightens. This was already noted in this object by Wamsteker et al. (1990), Clavel et al. (1991), and Peterson (1991). Using the best-fitting linear regression, we will assume that there is a *perfect* relation between the spectral index and the flux, and all of the observed scatter is attributable to observational error:

$$\alpha_{1800-4200} = (0.123 \pm 0.004)F_{1800} - (0.79 \pm 0.05)\,, \quad (1)$$

where F_{1800} is in units of 10^{-14} ergs s^{-1} cm^{-2} Å^{-1}. Using this relation and the observed F_{1800}, we can then measure the flux in the bump in *all* the *IUE* spectra with improved accuracy. (In the linear regression we have excluded the outlier from JD 2,447,742. This measurement is from a spectrum taken with a relatively narrow (1″.5) slit, in which flux-calibration problems in the blue are likely.)

It is important to verify that the relation in equation (1) is not an artifact. Such a relation could arise if in reality the spectral index were constant, but we underestimated the starlight contribution at 4200 Å. A constant starlight flux of 4.6×10^{-15} ergs s^{-1} cm^{-2} Å^{-1} at 4200 Å, which is 1.7 times the value we have assumed, would be needed to explain the effect. A relation similar to equation (1) can also be found if the 5100 Å continuum, rather than the 4200 Å continuum, is used. A constant starlight flux of 6.7×10^{-15} ergs s^{-1} cm^{-2} Å^{-1} at 5100 Å, that is, twice the value we have assumed, is then needed to explain the variation in spectral slope. However, Peterson et al. (1992) have measured a 5100 Å flux as low as 5.6×10^{-15} ergs s^{-1} cm^{-2} Å^{-1} during a faint state of NGC 5548, thus setting a firm upper limit on the amount of starlight at 5100 Å, and ruling out the above scenario.

Table 2 lists the epoch and small bump flux measured using equation (1) to determine the nonstellar continuum. In order to investigate the relative contributions to the variations of the two main components of the bump—the Fe II multiplet blends and the Balmer continuum—we separate our measurements in Table 2 to the two bands defined above, UV1 (from 2260 to 2655 Å) and UV2 (from 2655 to 3045 Å). Mg II λ2800 has again been subtracted from the UV2 measurement.

Figure 3 shows the light curves from Table 2. The top curve (the UV1 + 2 flux) reveals that the measurement using the functional relation for the spectral index (eq. [1]) has indeed removed much of the noise in the light curve of Table 1, and made apparent the variations in the small bump. The two components of the UV1 + 2 flux, UV1 and UV2, also shown in Figure 3, are qualitatively alike and have similar variation amplitudes relative to the mean fluxes. Since the contribution of the Balmer continuum is larger in the UV2 band (WNW), this suggests that both the Fe II blends and the Balmer continuum are varying with comparable amplitude and time scales.

To investigate this further, we have compared the variation amplitudes in the UV1 band and the OPT1 band (3245–3635 Å) and examined the relative contribution of Balmer continuum and Fe II emission in each band. Modeling of quasar spectra by WNW shows that at ~3600 Å practically all of the flux above the power-law continuum is Balmer continuum emission. We have scaled one of the WNW Balmer continuum models [$T = 10^4$ K, optical depth $\tau(\lambda 3646) = 2$] by varying amounts to account for the ~3600 Å flux above the best-fitting power law in the spectra that have uninterrupted wavelength

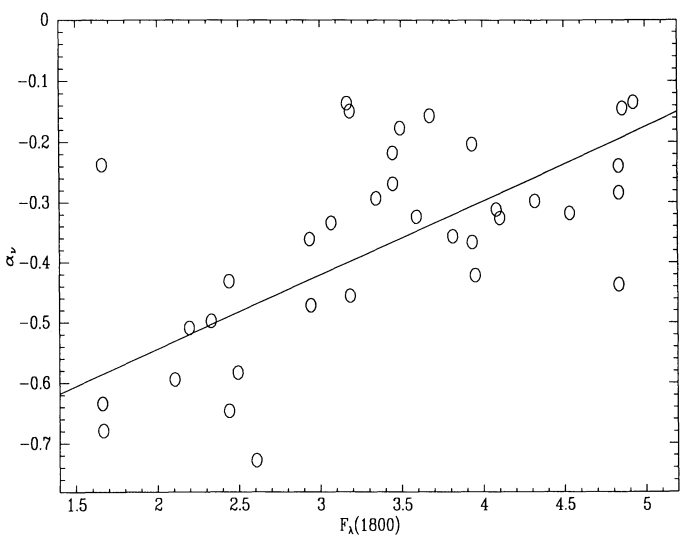

FIG. 2.—Relation between the power-law spectral index α_ν from 1800 to 4200 Å and the continuum flux at 1800 Å. Also shown is the best linear fit. F_λ is in units of 10^{-14} ergs s^{-1} cm^{-2} Å^{-1}.

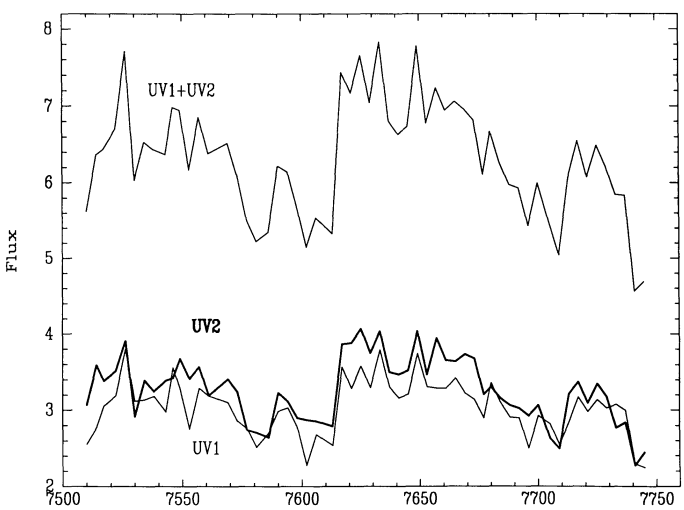

FIG. 3.—Light curve for the small blue bump flux in the UV1+2 band (2260–3045 Å; *top curve*), and in the UV1 and UV2 bands (*two bottom curves*), from Table 2. The flux is integrated above a power law determined by the continuum level at 1800 Å and a spectral index from the best-fit relation in Fig. 2. The Mg II λ2800 line flux has been subtracted from the total UV2 flux. Flux is in units of 10^{-12} ergs s^{-1} cm^{-2}.

TABLE 2

LIGHT CURVES

JD (−2440000)	F_λ(1800)	UV1 2260–2655 Å	UV2 2655–3045 Å	Total 2160–4130 Å
7510.....	3.06	2.55	3.06	11.2
7514.....	3.03	2.77	3.58	12.7
7517.....	3.24	3.05	3.38	12.8
7522.....	3.67	3.18	3.51	13.3
7526.....	3.59	3.79	3.90	15.4
7530.....	3.82	3.11	2.91	12.0
7534.....	3.64	3.13	3.39	13.0
7538.....	4.37	3.18	3.24	12.8
7543.....	4.54	2.97	3.39	12.7
7546.....	4.48	3.56	3.42	13.9
7549.....	3.95	3.27	3.67	13.8
7553.....	3.96	2.75	3.41	12.3
7557.....	3.49	3.28	3.56	13.7
7561.....	2.74	3.18	3.19	12.7
7569.....	2.59	3.10	3.41	13.0
7573.....	2.32	2.86	3.24	12.2
7577.....	2.19	2.76	2.74	11.0
7581.....	2.10	2.51	2.70	10.4
7586.....	2.49	2.70	2.64	10.6
7590.....	2.44	2.98	3.23	12.4
7594.....	2.39	3.03	3.11	12.2
7598.....	2.97	2.78	2.90	11.3
7602.....	3.37	2.27	2.87	10.3
7606.....	3.43	2.68	2.85	11.0
7613.....	4.10	2.53	2.78	10.6
7617.....	3.82	3.56	3.86	14.8
7621.....	4.83	3.28	3.87	14.3
7625.....	4.71	3.58	4.07	15.3
7629.....	4.85	3.29	3.74	14.0
7633.....	4.61	3.79	4.03	15.6
7637.....	4.51	3.30	3.50	13.6
7641.....	4.92	3.16	3.46	13.2
7645.....	4.53	3.21	3.52	13.4
7649.....	4.14	3.74	4.03	15.5
7653.....	4.31	3.30	3.46	13.5
7657.....	4.08	3.28	3.94	14.4
7661.....	3.93	3.28	3.65	13.8
7665.....	3.81	3.42	3.63	14.1
7669.....	3.46	3.22	3.73	13.9
7673.....	3.30	3.13	3.67	13.6
7677.....	3.16	2.90	3.20	12.2
7680.....	3.18	3.35	3.30	13.3
7684.....	2.91	3.10	3.15	12.5
7688.....	2.60	2.90	3.06	11.9
7692.....	2.60	2.90	3.02	11.8
7696.....	2.72	2.50	2.92	10.8
7700.....	2.69	2.92	3.06	11.9
7705.....	2.93	2.81	2.62	10.8
7709.....	3.34	2.54	2.49	10.0
7713.....	3.24	2.84	3.21	12.1
7717.....	3.44	3.17	3.37	13.0
7721.....	3.33	2.98	3.09	12.1
7725.....	2.94	3.13	3.34	12.9
7729.....	2.26	3.02	3.17	12.4
7733.....	1.86	3.07	2.76	11.6
7737.....	1.50	2.99	2.83	11.6
7741.....	1.65	2.29	2.27	9.12
7745.....	1.66	2.24	2.44	9.37

NOTES.—F_λ in units of 10^{-14} ergs s^{-1} cm^{-2} Å^{-1}. Fluxes in units of 10^{-12} ergs s^{-1} cm^{-2}.

coverage. This Balmer continuum model fits well the spectrum of several quasars (WNW) and is also similar in shape to a Balmer continuum model with $T = 2 \times 10^4$ K and small optical depth.

Of the total flux of the Balmer continuum model, 19% is in the UV1 band, 25% is in the UV2 band, and 33% is in the OPT1 band. The contribution of the Balmer continuum model to the small bump flux is ~25% in the UV1 band, ~40% in the UV2 band, and ~75% in the OPT1 band. The fractions are similar both for spectra with high and low OPT1 band fluxes, indicating that the other main component of the UV1 and UV2 bands, the Fe II emission, varies with comparable amplitude to the Balmer continuum. We plot in Figure 4 the OPT1 flux from Table 1 versus the UV1 flux from Table 2 for the *IUE* epoch closest in time. Although the number of points is small and the scatter is large, one sees again that the relative amplitudes of variation of the two components are similar. The lowest OPT1 point in Figure 4 is the measurement at JD 2,447,742, which we have already noted is probably flawed. If it is excluded, the ratio of the extreme values in the OPT1 band is 1.6. If the Fe II flux were constant, then a variation of at most 1.3 (maximum/minimum) would be expected in the UV1 band, as opposed to the 1.6 that we find, even while ignoring the extreme UV1 points. Conversely, the factor 1.6 variation observed in the UV1 band, if due solely to Balmer continuum variation, would cause a variation of factor 2.8 in the OPT1 band. Since our best estimate for the variation amplitudes is ~1.6 in both UV1 and OPT1 in all spectra having the two bands, we conclude that the Balmer continuum and Fe II emission are varying with similar amplitudes.

As a final step in our measurement process, we need to correct the bump flux measured in the *IUE* spectra to account for the unmeasured flux between 2160 and 2260 Å and 3045 and 4130 Å. The similar relative variation amplitudes we measure in various parts of the bump justify using a constant multiplicative factor for this correction. By comparing the total bump flux (2160–4130 Å) in each of the 13 optical spectra going down nearly to 3200 Å to the UV1+2 flux from Table 2 in the nearest *IUE* spectrum, we obtain a correction factor of 1.99 ± 0.16. The fifth column of Table 2 gives the sum of the previous two columns times this correction factor and is our best estimate for the flux of the small blue bump as a function of time. Figure 5 shows the final light curve from column (5) of Table 2. For comparison, we superpose a scaled version of the 1350 Å continuum flux from Clavel et al. (1991).

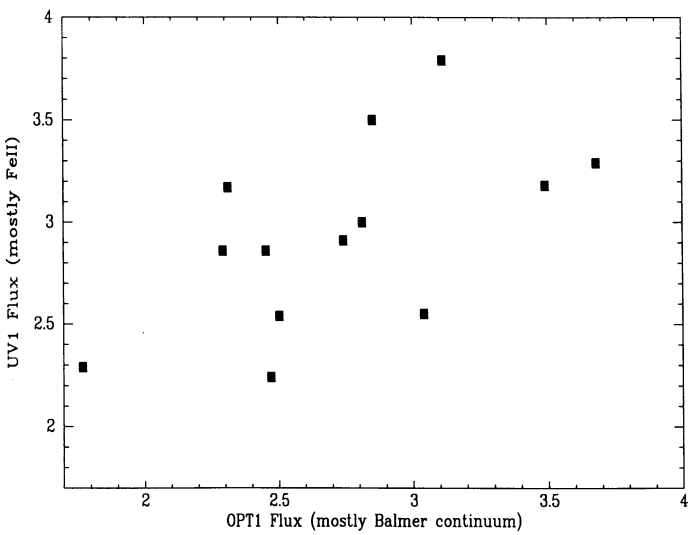

FIG. 4.—UV1 flux, which is dominated by Fe II emission, plotted against the OPT1 flux, which is almost entirely Balmer continuum emission. The two bands display similar variation amplitudes, indicating that both the Fe II emission and the Balmer continuum vary with similar relative amplitudes. Flux is in units of 10^{-12} ergs s^{-1} cm^{-2}.

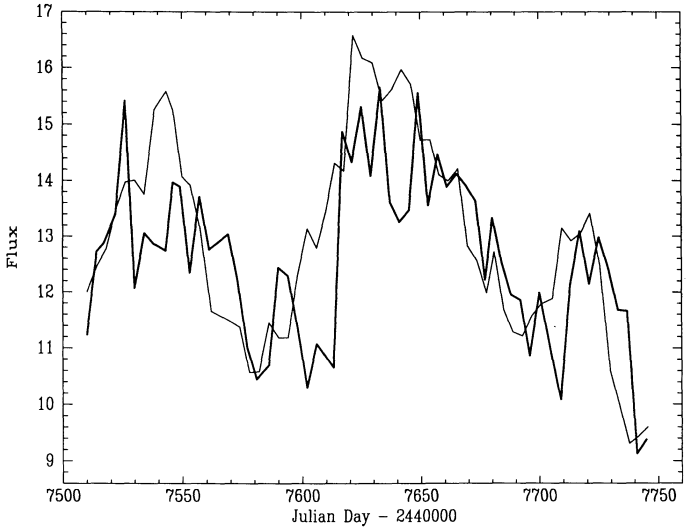

FIG. 5.—Final light curve for the small blue bump in NGC 5548, obtained by scaling the UV1+2 light curve in Fig. 4 by a factor of 2.0. Flux is in units of 10^{-12} ergs s^{-1} cm^{-2}. The thin line is a scaled version of the 1350 Å continuum light curve. The small blue bump is, like most other emission features in NGC 5548, strongly correlated with the continuum, with a lag of ~10 days.

The unknown observational uncertainties in much of the data used here, plus the complicated iterative process we have used to arrive at our final light curve, make it pointless to attempt to analytically derive error estimates. Instead, we use an empirical approach of comparing adjacent measurements (i.e., separated by ~4 days) to obtain the scatter from point to point (Peterson et al. 1991, 1992). This method assumes that there are no line variations on time scales of 4 days. The point-to-point variations that result from long-time-scale trends in the light curve will cause this method to give an overestimate of the uncertainty. We find that the errors on the measurements in Table 2 are ±10%.

An additional systematic source of uncertainty is associated with the measurement process itself, for example, the assumption that the underlying continuum has a power-law form and the choice of points used to set the power law. To assess the importance of this assumption, we have repeated the measurement process setting the long-wavelength continuum point at 5100 Å rather than at 4200 Å. The resulting small bump light curve is very similar to that of Figure 5. If, in addition, 1350 Å rather than 1800 Å is used to determine the short-wavelength continuum point, the resulting light curve has a mean flux and variation amplitude that are increased by ~25% relative to Figure 5. We suspect that this increase is due to the inclusion of continuum flux in the small bump measurement; the 1350 Å continuum is generally lower than the extrapolation of a power law passing through the 1800 Å window (see Fig. 1). By using continuum windows that are as close as possible to the bump itself, we are minimizing both the contamination by continuum flux to the bump and the effect of assuming a particular (power-law) shape for the underlying continuum. If, instead of a power-law continuum, a thin accretion-disk model spectrum (Laor & Netzer 1989) passing through the 1800 and 4200 Å windows is used, the small bump flux in a typical NGC 5548 spectrum is reduced by ~20%.

A related issue is that of reddening, both Galactic and internal. As discussed by Wamsteker et al. (1990), the amount of reddening in NGC 5548 is small, but uncertain. Following Clavel et al. (1991) and Peterson et al. (1991), we choose not to correct the measurements for reddening at this time. If, as indicated by the above measurements, the shape of the small blue bump is constant with time (i.e., only its amplitude varies), the reddening correction is simply a multiplicative constant which may be applied retroactively to the fluxes in Table 2. For example, a correction for Galactic reddening with $E_{B-V} = 0.05$ mag would increase the small bump fluxes by ~30%.

3. ANALYSIS AND DISCUSSION

In this section we carry out a simple time-series analysis of the small bump light curve, similar to that carred out by Clavel et al. (1991), Peterson et al. (1991), and Dietrich et al. (1992) for the other emission lines of NGC 5548.

It is clear that the small blue bump shows the same three "events" that characterize the light curves of the continuum and most of the other emission lines and exhibits a delay relative to the continuum variations. A cross correlation of the small bump with the 1350 Å continuum has a peak with a correlation coefficient of 0.80 at a lag of 6 days (thick line in Fig. 6). Its centroid is at 9 days lag. This is similar to the lag found by Clavel et al. (1991) for Lyα and C IV λ1549. In fact, the light curves of Lyα and the small bump are quite similar; cross-correlation of the two has a peak correlation coefficient of 0.68 at 0 days lag (thin line in Fig. 6).

To estimate the uncertainty in the lag of the small bump, we have carried out Monte Carlo simulations as described by Gaskell & Peterson (1987) and Maoz & Netzer (1989). A smoothed version of the observed continuum light curve was convolved with the response of thin-shell BLR geometries of various sizes. The thin shell geometry is probably a poor representation of the BLR of NGC 5548, but it suffices in order to estimate the uncertainty in the cross-correlation lag, since it generates a simulated emission-line light curve with the required temporal characteristics (see Maoz & Netzer 1989). The response of each BLR cloud to the ionizing flux impinging on it was assumed to be instantaneous. This is a good approx-

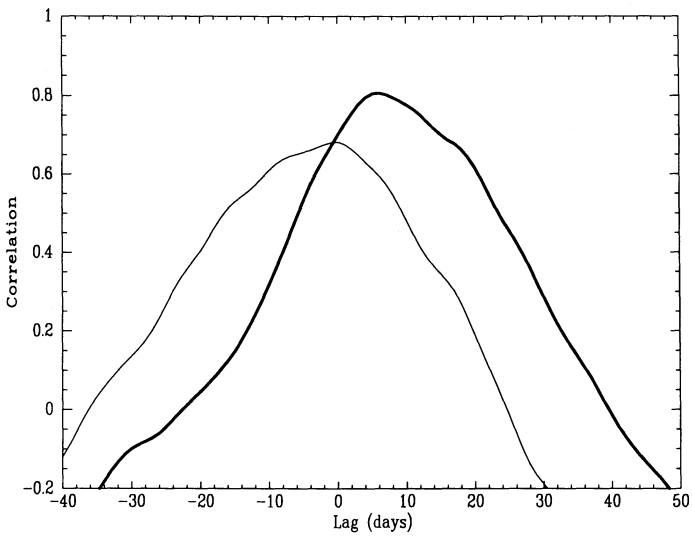

FIG. 6.—Cross-correlation functions of the small blue bump vs. the 1350 Å continuum (*thick line*) and vs. Lyα (*thin line*).

imation since, with a BLR electron density of 10^9 cm^{-3} or larger, the recombination time is 1 hr or less. The resonance-line photon diffusion time for BLR conditions is of order 100–1000 s. The cloud response time is thus much shorter than the light travel time across the BLR, which we have found to be of order a week. The simulated continuum and emission-line light curves were then sampled with a sampling grid of 4 days, and Gaussian-distributed errors of appropriate size were applied. The light curves were cross-correlated, and the centroid of the cross-correlation function found. This process was repeated many times to obtain the distribution of cross-correlation peaks for each assumed geometry. We find that the uncertainty in the lag as a result of sampling and random measurement errors is of order 1–2 days. Another source of uncertainty in the lag is the systematics of the measurements process itself. We have repeated the bump measurements letting the parameters in equation (1) vary within their range of uncertainty. This induces a change in the lag of $\sim \pm 1$ day.

We conclude from this that the peak response of the small bump emission arises physically in the same region as that of the other main lines. This is consistent with the finding by Boroson & Green (1992) that the optical Fe II blends in PG quasars have the same broadening as Hβ, suggesting they come from the broad-line region like the other emission lines. The peak-to-peak variation amplitude of the small bump relative to the mean value is $\sim \pm 20\%$, similar to the Balmer lines measured by Peterson et al. (1991) and Dietrich et al. (1992), and considerably smaller than the relative variation in Lyα and C IV λ1549 (Clavel et al. 1991).

Wamsteker et al. (1990) analyzed combined *IUE*/optical data of NGC 5548 for a range of continuum levels similar to that observed during the 1988–1989 monitoring campaign (but with far fewer epochs spread over 8 yr). They fitted the small blue bump with models for the Balmer continuum and the Fe II blend and found that all the variations in the bump were consistent with being due to the Balmer continuum while Fe II stayed constant. They also found that the amplitude of the Balmer continuum variations was comparable to, and perhaps even larger than, that of Lyα. Both of these results are in disagreement with our results here: we find that the blue bump varies by a factor of 1.6 (maximum/minimum) while Lyα varies by a factor of 2, and we find that both Fe II and the Balmer continuum contribute comparably to these variations.

To investigate the source of this disagreement we applied the analysis described in this paper to several of the spectra that were used by Wamsteker et al. in their analysis. In particular, we tried to see whether or not, for similar continuum levels to those observed in the 1988–1989 campaign, we measure similar bump fluxes in the UV1 and UV2 ranges. The results are mixed: a "low state" spectrum from 1981 July has bump fluxes in these two ranges that are similar to those we measure in 1989 for comparable continuum levels; a 1982 March "high-state" spectrum has the same UV1 flux that we measure in the 1989 high states, but its UV2 flux is indeed 1.5 times higher than in 1989. These two spectra would suggest that, in fact, the Balmer continuum responded more strongly in the past to continuum outbursts. Since the earlier data have very poor temporal resolution, it is also possible that the strong Balmer emission seen then is the response of an extended BLR component to a prolonged high state, a component that had no time to respond to the relatively short outbursts of 1988–1989. However, the picture becomes more complicated when other old spectra are examined. For example, an "intermediate state" spectrum from 1984 February has similar flux to one of the 1989 campaign spectra (JD 2,447,534) between 1150 and 2300 Å. Then, from 2300 to 3200 Å, it is higher by $\sim 15\%$ than the 1989 spectrum. As a result, the bump flux in the UV1 band is 1.5 times higher than in the 1989 spectrum, while in the UV2 band it is only slightly higher than in 1989. This spectrum thus shows an opposite effect to that seen in the 1982 March spectrum. A 1984 May "high-state" spectrum has UV1 and UV2 fluxes 1.9 and 1.6 times larger than measured in 1989 for the same continuum levels.

We conclude that the differences in our results and those of Wamsteker et al. (1990) are not due to the different methods of analysis, but to real differences in the data. It is unclear to us whether the source of the differences is instrumental, or whether the small bump actually had a different response in 1988–1989 than in some past years, or if the differences are due to a combination of these effects. Whatever is the case, the frequent sampling, the large number of observations, and the uniformity with which they were carried out, make the 1989 campaign data more suitable for determining the behavior of the small blue bump in NGC 5548.

To summarize, we have used an iterative method to measure the light curve of the "small blue bump" in NGC 5548 from *IUE* and ground-based observations obtained in 1988–1989. In order to subtract the nonstellar continuum underlying this blend of emission lines, our scheme makes use of the empirical result that the continuum hardens as it brightens. The small blue bump has a light curve which, like most of the other emission lines of NGC 5548 monitored in 1988–1989, reflects the three continuum outburst events that took place. The flux in the bump lags the continuum events by ~ 10 days, similar to Lyα, but its variation amplitude is smaller and more like that of Hβ. Different parts of the bump vary with similar relative amplitude, which indicates the two main components of the bump—the Balmer continuum and the blend of Fe II UV multiplets—are both variable. These results suggest that the Balmer continuum and Fe II emission are emitted in the broad-line region. Since about one-third of the total line flux is in it, the small blue bump is the single most important line cooling feature in NGC 5548, and its behavior needs to be accounted for by any model for the line emission of this object.

We thank G. Reichert and P. Rodriguez for their help in accessing the *IUE* data. H. N. and B. M. P. thank the Institute for Advanced Study for its hospitality in the course of this work. We are also grateful to the following individuals, who contributed data that were used in this study: A. Cochran, R. Cohen, K. Fricke, M. Penston, E. Perez, R. Pogge, M. Richmond, and S. Veilleux. We also thank the referee, R. Puetter, for his comments and suggestions. This work was supported by NASA grant NAG5-1366 to Ohio State University (B. M. P.), a senior NRC fellowship at NASA/Goddard and US-Israel Binational Science Foundation grant 89/00179 (H. N.), NSF grants AST-8957063 and AST-9003829 (A. V. F.), NSF grants AST-9058510 and RII-8800660 (J. B.), and NASA contract NAS 5-29293 (P. S. S.).

REFERENCES

Bahcall, J. N., Kozlovski, B., & Salpeter, E. E. 1972, ApJ, 171, 467
Blandford, R. D., & McKee, C. F. 1982, ApJ, 255, 419
Boroson, T. A., & Green, R. F. 1992, ApJS, 80, 109
Clavel, J., et al. 1991, ApJ, 366, 64
Dietrich, M., et al. 1993, ApJ, in press
Gaskell, C. M., & Peterson, B. M. 1987, ApJS, 65, 1
Horne, K., Welsh, W. F., & Peterson, B. M. 1991, ApJ, 367, L5
Johnson, H. M. 1979, ApJ, 230, L137
Krolik, J. H., Horne, K., Kallman, T. R., Malkan, M. A., Edelson, R. A., & Kriss, G. A. 1991, ApJ, 371, 541
Laor, A., & Netzer, H. 1989, MNRAS, 238, 897
Maoz, D., & Netzer, H. 1989, MNRAS, 236, 21
Miller, J. S., & Stone, R. P. S. 1987, The CCD Cassegrain Spectrograph at the Shane Reflector (Lick Obs. Technical Report 48)
O'Connell, R. W. 1980, ApJ, 236, 430
Peterson, B. M. 1991, in Variability of Active Galaxies, ed. W. J. Duschl, S. J. Wagner, & M. Camenzind (Heidelberg: Springer), 47
Peterson, B. M., et al. 1991, ApJ, 368, 119
———. 1992, ApJ, 392, 470
Reichert, G., et al. 1991, in Variability of Active Galactic Nuclei, ed. H. R. Miller & P. J. Wiita (Cambridge: Cambridge Univ. Press), 335
Wamsteker, W., et al. 1990, ApJ, 354, 446
Wanders, I., Peterson, B. M., Pogge, R. W., DeRobertis, M. M., & van Groningen, E. 1992, A&A, in press
Wills, B. J., Netzer, H., & Wills, D. 1985, ApJ, 288, 94 (WNW)